Parametric Numerical Study of the Flow and Heat Transfer in Microchannel with Dimples

Minghai Xu[1], Hui Lu[1], Liang Gong[1,*], John C. Chai[2], Xinyue Duan[1]

[1]Shandong Province Key Laboratory of Oil&gas Storage and Transportation Safety China University of Petroleum (East China), Qingdao Shandong, PRC, 266580

[2]Department of Engineering and Technology, School of Computing and Engineering, University of Huddersfield, Huddersfield, HD1 3DH, UK

[*]Corresponding author Email: lgong@upc.edu.cn

ABSTRACT

The characteristics of flow and heat transfer in microchannel with dimples were numerically investigated. The geometric parameters of dimpled channel, including aspect ratio, dimple depth and dimple spacing, were independently studied under constant Reynolds number 500. A constant heat flux 1W/mm^2 was adopted in the central area at the bottom of the microchannel heat sink to simulate a high power device. In comparison to straight channels, dimpled surface reduced the local flow resistance and also improved thermal performance of micro-channel heat sink. Compared to flat channel case, the optimal dimpled case have 3.2K decrease of temperature, 15% gain of Nusselt number and 2% reduce of pressure drop.

Key words: *dimple, microchannel, flow drag reduction, thermal performance, electronics cooling*

1. INTRODUCTION

Miniaturizations of integrated circuits (ICs) are facing many difficult challenges including packaging, line width, materials and etc. One of the most serious challenges is to manage the high thermal power density and to control temperature. According to the 2012 International Technology Roadmap for Semiconductors (ITRS), the maximum power density of a single-chip with high performance and multiple purpose units (MPU) will reach 1 W/mm^2 by the end of 2020 [1].

Traditional forced air convection cooling cannot manage such high heat flux without large radiators and powerful fans; which may result in unacceptable noise level and difficulty in system integration. Liquid cooling method with microchannels, separating the heat absorption from ICs and heat dissipation to air, has higher efficiency and high degree of integration. It will be an important option for cooling the next generation electronics.

In 1981, Tuckerman and Pease [2] built the first microchannel heat sink and proved its huge potential for IC cooling. Since their pioneering work, many studies on friction factors and Nusselt numbers in flat channels have been reported [3-8]. These works showed that the Navier-Stokes equations are still valid for these micron level channels. The axial heat transfer, surface roughness, viscous heating are also negligible. Wavy channel [9-12], branched channel [13-15], ribs, fins or rough elements [16-19] (such as triangular, rectangular, dimple elements and so on) have also been investigated, the rough elements method can strengthen the convection heat transfer without large pressure penalty and is a possible low-cost solution.

Jonghyeok Lee and Kwan-Soo Lee [20] studied plate heat exchanger with dimples and protrusions. The Reynolds numbers were varied from 500 to 15000. A genetic algorithm was used to determine the optimal dimple and protrusion shape. The optimal design enhances the performance factor by as much as 28% and is independent of Reynolds number. Alshroof et al. [21] investigated laminar flow (Reynolds number of 1600) and heat transfer of single dimple, single protrusion and their combinations. With a single dimple, a 9% increase in the performance factor was obtained. This was achieved with a 7% heat transfer enhancement and a 1.5% decrease in the average shear stress. With a single protrusion application, the performance factor increased by 32% even with higher average shear stress. Bi et al. [22] numerically studied the heat transfer in 1mm hydraulic diameter channel with dimples, cylindrical grooves and low height fins for Reynolds numbers from 2700 to 6100. It was concluded that, when the Reynolds number is larger than 3323, the dimpled channel has the best overall performance. They also concluded that the dimple

diameters and spacings can be optimized to increase performance. Wei et al. [23] studied steady laminar flow and heat transfer inside a microchannel with one dimple using periodic boundary conditions, the results show that the dimple could reduce the pressure drop under low Reynolds number. Lan et al. [24] studied rectangular microchannel with dimples and protrusions with Reynolds number from 100 to 900, for the dimple-only case they also find the dimple could reduce the reduce the pressure drop under low Reynolds number.

Ge et al. [25] studied the cosine-shaped dimpled heat sink with Reynolds number from 50 to 3000. They concluded that transition from laminar to turbulent flow begins at Reynolds number of 1000 and the flow becomes fully turbulent around Reynolds number of 3000. Lienhart et al. [26] reported experimental measurements and numerical simulations for turbulent flow over shallow (dimple depth to dimple print diameter ratio of 0.05) dimpled surfaces. Both in internal and external flow, the drag force consists of shear stress and pressure force didn't decrease. Though the shear stress was marginally decreased, the pressure force caused by dimples overcame these reduction, dimples couldn’t decrease the flow resistance. Turnow et al. [27] carried out experimental measurements and large eddy simulations on staggered dimpled surfaces for Reynolds numbers of 6521 and 13042. Ninety-three percent heat transfer enhancement and fourteen percent decrease in pressure drop was the best overall performance obtained with dimple depth to dimple print diameter (diameter of dimple edge) ratio of 0.26. Isaev et al.[28] presented numerical solutions for single dimple in narrow channel. The Reynolds number was varied from 20000 to 60000. The average Nusselt number enhancement was independent of Reynolds number. When both heat transfer enhancements and pressure losses were considered, the overall performance was better at lower Reynolds numbers. Tay et al. [29] conducted experiments on dimpled microchannels with dimple depth to dimple diameter ratios from 0.05 to 0.5. Flows were visualized by injecting dye into the flow passages. The Reynolds number was varied from 1000 to 28000. Six different flow stages

were observed when Reynolds number was growing. The flow stages development achieved under lower Reynolds number as the dimple's depths increase.

Silva. et al. [30] reviewed published literature on heat transfer enhancement with dimples for cooling of microelectronics. They concluded that heat transfer enhancements (1) are independent of the Reynolds number in laminar and transition flows, (2) are better at low Reynolds number due to the small pressure drop, (3) are better with shallow dimple (dimple depth to dimple diameter ratio of 0.2) and (4) can be optimized by properly spaced dimples placements

Xie et al. [31] presented numerical solutions of turbulent flows through microchannels with tear drop dimple and protrusion. It was concluded that tear drop dimple and protrusion enhanced heat transfer better than hemispherical dimple or protrusion, albeit with higher flow resistance. Yoon et al. [32] reported results from direct numerical simulations of flow through microchannels with tear drop dimple for a Reynolds number of 2800. It was concluded that a 4% heat transfer enhancement was obtained with the use of tear drop dimples.

From the above, majority of the available studies focused on turbulent flows, transition flows or higher spectrum of laminar flows. Micro channel heat sink used for electronic cooling must be highly reliable. As the leakage of fluid or failure of structure will damage the electronic or even the whole system. Thus properly designed cooling arrangements with laminar flow which has low pressure drop and higher efficiency may be more suitable for electronic cooling. The objective of this article is to study the effectiveness of cooling facilities utilizing dimples to enhance performance. The flow is kept laminar with a Reynolds number of 500. The effects of channel aspect ratios, dimple sizes and dimple arrangements are numerically studied to find the effect of dimple and a proper way to control the maximum temperature of electronics.

2. GEOMETRY MODEL

Fig. 1 shows the schematic of the microchannel heat sink considered in this article. Cooling is provided by flowing water through the fluid zone in the 1 mm $\times$ 1 mm $\times$ 20 mm (outer

dimensions) heat sink with dimples along the bottom of the fluid zone. There is a 10 mm heat source (Fig. 1b) in the middle of the bottom surface with a constant heat flux 1W/mm^2. As a result, the 5 mm upstream and 5 mm downstream sections of the bottom wall are unheated. The first dimple is placed 2 mm from the entrance and there are a total of 9-21 dimples in the channel depending on dimple spacing *s*.

The effects of the flow area aspect ratios (Fig. 1c), the dimple spacings (Fig. 1d) and the dimple depths (Fig. 1e) are examined in this article. Four flow area aspect ratios (width/height) namely, 1, 2, 3 and 4 are considered as shown in Fig. 1c. Dimple spacings *s* of 0.7 mm, 1.0 mm, 1.2 mm, 1.6 mm and 2.8 mm are studied. Dimple depths *d* of 0.05 mm, 0.1 mm, 0.15 mm and 0.2 mm are evaluated. The dimple diameter is kept at 0.2 mm.

3. GOVERNING EQUATIONS AND BOUNDARY CONDITIONS

The governing equations for steady, incompressible laminar flow of Newtonian fluid with constant properties are

Continuity Equation

$$\frac{\partial u}{\partial x}+\frac{\partial v}{\partial y}+\frac{\partial w}{\partial z}=0 \tag{1}$$

Momentum Equations

$$\frac{\partial(uu)}{\partial x}+\frac{\partial(vu)}{\partial y}+\frac{\partial(wu)}{\partial z}=\nu\left(\frac{\partial^2 u}{\partial x^2}+\frac{\partial^2 u}{\partial y^2}+\frac{\partial^2 u}{\partial z^2}\right)-\frac{1}{\rho}\frac{\partial p}{\partial x} \tag{2}$$

$$\frac{\partial(uv)}{\partial x}+\frac{\partial(vv)}{\partial y}+\frac{\partial(wv)}{\partial z}=\nu\left(\frac{\partial^2 v}{\partial x^2}+\frac{\partial^2 v}{\partial y^2}+\frac{\partial^2 v}{\partial z^2}\right)-\frac{1}{\rho}\frac{\partial p}{\partial y} \tag{3}$$

$$\frac{\partial(uw)}{\partial x}+\frac{\partial(vw)}{\partial y}+\frac{\partial(ww)}{\partial z}=\nu\left(\frac{\partial^2 w}{\partial x^2}+\frac{\partial^2 w}{\partial y^2}+\frac{\partial^2 w}{\partial z^2}\right)-\frac{1}{\rho}\frac{\partial p}{\partial z} \tag{4}$$

Energy Equation

$$\frac{\partial(uT)}{\partial x}+\frac{\partial(vT)}{\partial y}+\frac{\partial(wT)}{\partial z}=\frac{\lambda}{\rho c_p}\left(\frac{\partial^2 T}{\partial x^2}+\frac{\partial^2 T}{\partial y^2}+\frac{\partial^2 T}{\partial z^2}\right) \quad (5)$$

where ρ is the fluid density, *x* is the axial coordinate, *y* is the transverse coordinate, *z* is the transverse coordinate, *u* is the axial velocity, *v* is the transverse velocity, *w* is the transverse velocity, ν is the fluid viscosity, *p* is the pressure, c_p is the fluid specific heat and λ is the thermal conductivities of the fluid and heat sink material.

Boundary Conditions

***Inlet*:** The inlet Reynolds number (based on the hydraulic diameter) Re is set to 500 and the inlet temperature is kept at 300K.

***Outlet*:** Zero axial gradients of the transverse velocities and temperature are specified at the outlet. The axial velocity is calculated to ensure mass conservation.

***Bottom Wall*:** No slip condition is imposed on the velocities. The heat flux on the 10mm long heat source starting at *x* = 5 mm is specified as 1 W/mm2. The remainder of the bottom wall is adiabatic.

Other Walls: No slip condition is imposed on the velocities. All walls are assumed adiabatic.

The specific heat capacity of water C_p = 4.2 kJ/kg·K, the thermal conductivity of water λ_f = 0.6 W/m·K, the density of water ρ_f=998.2 kg/m^3 and the dynamic viscosity of water μ_f=1.003×10^{-3} Pa·s. The solid material of microchannel is copper with a thermal conductivity λ_s=297 W/m·K.

4. AUXILIARY PARAMETERS

The average Nusselt number, the local Nusselt number, the thermal resistance and the performance factor are used to evaluate the effectiveness of the dimpled heat sink. These parameters are defined in this section.

The average Nusselt number is calculated as

$$Nu = \frac{hD_e}{\lambda_f} = \frac{QD_e}{A_{wall}\lambda_f\left(T_{wall} - T_f\right)} \tag{6}$$

$$D_e = \frac{4Ac}{P} \tag{7}$$

$$A_{wall} = 2L\left(H_w + H_c\right) + \frac{n}{3}\pi d^2\left(3r - d\right) - 2n\pi\sqrt{r^2 - \left(r - d\right)^2} \tag{8}$$

$$T_{wall} = \frac{\iint_{wall} TdA}{A_{wall}} \tag{9}$$

$$T_f = \frac{\iiint_{fluid} TdV}{\iiint_{fluid} dV} \tag{10}$$

Where D_e is the hydraulic diameter, Q is the total heating power(=10 W). A_{wall} is the area of fluid solid interface. T_{wall} and T_f is average temperature of fluid solid interface and fluid.

In Eq. (7), A_c is the inlet cross-sectional area of the flow channel and P is the wetted perimeter of the flow channel at the inlet. In Eq. (8), L is the channel length, H_w is the flow channel width, H_c is the flow channel height, n is the number of dimple, d is the dimple depth and r is the dimple radius.

The local Nusselt number at a point P at position (x, y, z) on the wall is calculated through:

$$Nu_P = \frac{h_P D_e}{\lambda_f} = \frac{\lambda_s}{\lambda_f}\frac{D_e}{\left(T_P - T_x\right)}\left|\left(\frac{\partial T}{\partial n}\right)_P\right| \tag{11}$$

$$T_x = \frac{\iint_{A_x} \rho c_p uTdA}{\iint_{A_x} \rho c_p udA} \tag{12}$$

where $\left(\frac{\partial T}{\partial n}\right)_P$ is the temperature gradient normal to the fluid-solid interface (solid side). T_x is the cross-sectional average temperature of fluid at positon x and T_P is the local wall temperature.

Total thermal resistance including conduction resistance and conduction resistance is calculated using equation below, average temperature of heating surface $T_{heat}$and fluid T_f is heat flux weighted:

$$R = \frac{T_{heat} - T_f}{Q} = \frac{\iint_{heat} Tqds - \iiint_{fluid} T\lambda_f \mathrm{div}(\mathbf{grad}T)dv}{Q^2} \tag{13}$$

The performance factor PF 18[9] is a measure of the ratio of the heat transfer enhancement and the penalty on the pressure drop between the dimpled channel and the flat channel. It is defined as

$$PF \equiv \left[\frac{Nu / Nu_0}{(\Delta p / \Delta p_0)^{1/3}} \right]_{Re} \tag{14}$$

where Δp is the difference of average pressure between the inlet and the outlet, p_{in}-p_{out}, Nu is defined in Eq. (6) and the subscript 0 stands for flat channel heat sink with the same inlet aspect ratio.

5. RESULTS AND DISCUSSION

5.1. Mesh Independency Check

Hexahedral meshes (Fig. 2) were used in this study. Equations are solved by SIMPLE algorithm. Carefully grid independency check was carried out for each case separately. As an example, Fig. 3 shows the grid independency check for flat channel heat sink with aspect ratio 1:1. The differences in the average Nusselt number (Eq. 6) and pressure drop between the inlet and outlet are within 0.5% when the number of control volumes are doubled from 3.41 million to 7.87million. In this situation, 3.41 million control volumes were used for all simulations. Finally, 3.41 million, 4.38million, 5.69 million and 7.12 million control volumes were used for 1:1, 2:1, 3:1 and 4:1 aspect ratios respectively.

5.2. Effect of Aspect Ratio

Four different channel width to channel height ratios namely, 1:1, 2:1, 3:1 and 4:1 as shown in Fig. 1c are studied. For proper comparisons, the dimples' depth and spacing are unchanged in this study. Starting at 2mm from the entrance, 21 dimples are placed at the bottom of channel 0.7mm

(center-to-center distance as shown in Fig. 1d) apart. The dimples' radius and depth are 0.2 mm and 0.1 mm respectively.

As the aspect ratio increases, the flow cross-sectional area decreases. As the Re is kept constant at 500, the average velocity at every cross-section increases with aspect ratio. Therefore, we expect higher Nu, lower heat sink temperature and higher pressure drop with increasing aspect ratios.

Table shows the average Nusselt numbers Nu, overall average pressure drops (between inlet and outlet)Δp, maximum heat sink temperatures $T_{max,}$ The average Nusselt numbers for flat channels Nu_0 and pressure drops for flat channels Δp_0 are also tabulated for comparisons.

For the Reynolds number considered, dimples have positive effects on both heat transfer enhancements and pressure drops. Without dimples, the average Nusselt number increases by 1.35% (from 8.12 to 8.23) as the aspect ratio changes from 1:1 to 4:1. With dimples, the average Nusselt number increases by almost 15% (from 8.21 to 9.44) for the same changes in the aspect ratios. With dimples, the average pressure drops is lower by around 2%. With dimples, some fluid is trapped inside the dimples. As a result, recirculation zones are formed at the leading edges of the dimples. The velocities on top of these recirculation zones which are non-zero and positive are in contact with the through flow above the dimples. As a result, unlike without dimples where the fluid velocity at the wall is zero due to the no-slip condition, the through flow velocities alternates between zero and non-zero; non-zero when it flows over a dimple and zero when it is in contact with the flat bottom surface. This leads to lower pressure drops with the addition of dimples.

With dimples, the performance factor PF increases between 2% to 16% with aspect ratios. As expected, the maximum temperature of the heat sink also decreases with aspect ratios.

Fig. 3 shows the surface limited streamlines on the bottom wall of the channel showing the flow patterns inside one of the dimples (x=10mm). The flow is from left to right and the upstream most point of the plot is 5 mm into the heated section or 10 mm from the inlet of the problem. It is

seen that as the aspect ratio increases, the recirculation zones spread to cover the whole surface of the dimple. This implies that the through flow is in contact with a forward moving trapped fluid in the recirculation zone over the majority of the dimple opening. This reduces the velocity gradient experienced by the through flow and thus reduces the losses due to frictional forces leading to a reduced pressure drop (compare to the flat bottom surface heat sink).

Fig. 5 shows the streamline in dimple. We can clearly see the status of vortex and flow separation. While the d/H_c grows, the re-attach point moves downstream, but still in the dimple. The flow separation area is growing with d/H_c. In the case of aspect ratio 4:1 the flow separation occupies most part of the dimple surface. The vortex in the dimple changes greatly when d/H_c grows. In aspect ratio 1:1 channel, vortex is quite uniform in the dimple. But in the case of aspect ratio 2:1, the vortex begins to separate to two symmetrical vortexes and the center of vortex begin to move to side of the dimple. In the case of aspect ratio 4:1, the vortex is apparently stronger than that in the case of aspect ratio 1:1. And the vortex becomes two symmetrical parts. The axis of vortex near the wall is already vertical. These vortexes caused by the dimples can decrease the viscous dissipation due to the velocity gradient control (will be analyzed in next section), but the most important impact of dimples is the flow convection normal to flow direction, which is caused by periodic placement of dimples. As shown in Fig. 6, fluid is moving in twists and turns. With the increase of channel aspect ratio, the convection becomes stronger and developing into two opposite direction swirling. These phenomena mix the different layer of fluid in laminar flow and enhance the heat transfer in fluid, which is the main reason of heat convection resistance reduction.

Local Nusselt number near the dimple located in the middle of the channel (x=10mm) is shown in Fig. 7. The area with higher local Nusselt number appears in the flow reattachment area and where the cooler fluid moves towards the wall in Fig. 6. With the vortex status change and transverse convection change under different aspect ratio, the high local Nusselt number area also changes. In high aspect ratio case, high Nusselt number area split into two symmetry area in the

downstream of the vortex. The maximum value of local Nusselt number can reach 65 in 4:1 channel, compared to only 35 in 1:1 channel.

Increasing aspect ratio is apparently beneficial to the heat transfer in microchannel, while fluid velocity increase near the wall in high aspect ratio structure is the main reason of vortex strengthening and heat transfer enhancement.

5.3. Effect of Dimple Depth

Based on aspect 4:1 model, different dimple depth is taken into account to study the effect. Part of the data are listed in Table .

In Table , the pressure drop is apparently decreasing with dimple depth growing, and the maximum decrease is 3.8%. Relation between thermal resistance and dimple depth is parabolic: thermal resistance decreases first and then increase. Among the present cases, case with dimple depth 0.1 has the minimum thermal resistance. Same as the influence of dimple on pressure drop, the influence of dimple on heat transfer is also weak: the maximum temperature difference between four cases is only 1.27K, demonstrating that changing the dimple depth does not have important impact.

Average viscous dissipation rate on cross section along *x* direction is plotted in Fig. 8 and Fig. 9. Viscous dissipation rate of incompressible viscous flow could be calculated by equation below:

$$\Phi = \mu\left[2\left(\frac{\partial u}{\partial x}\right)^2 + 2\left(\frac{\partial v}{\partial y}\right)^2 + 2\left(\frac{\partial w}{\partial z}\right)^2 + \left(\frac{\partial u}{\partial y} + \frac{\partial v}{\partial x}\right)^2 + \left(\frac{\partial v}{\partial z} + \frac{\partial w}{\partial y}\right)^2 + \left(\frac{\partial w}{\partial x} + \frac{\partial u}{\partial z}\right)^2\right] \quad (15)$$

In the flat case, the viscous dissipation rate is constant after the entry effect. In the cases with dimples, the viscous dissipation rate dives when velocity gradient decrease (caused by low velocity vortex) and increases again because of the flow reattachment. Though the viscous dissipation rate reduces in the dimple; but the volume growth will counterbalance the total viscous dissipation. When dimple depth equals 0.2mm, the flow passage volume gained 28.13% compared

to flat channel. While average viscous dissipation rate decreases 26.2% and the pressure drop only decreases 3.92%. Streamline in the dimple in Fig. 10 indicates that the vortex variation with dimple depth is similar to impact of aspect ratio: d/H_c plays an important role in the vortex develop. d/H_c below 0.6 lead to a single vortex in the dimple and d/H_c above 0.6 lead to two symmetry vortexes. The transverse convection status also depends on the d/H_c. As shown in Fig. 11 the swirling is always symmetric. There are two symmetric swirling with opposite rotating direction when d/H_c stays below 0.6. When d/H_c is set above 0.6, these two swirling break up to four swirling. With the d/H_c grows, two swirling in the middle grow stronger, while two swirling on the side become weaker. The status of swirling stop change with d/H_c when d/H_c >1.2.

Local Nusselt number are listed in Fig. 12. It shows that dimple depth 0.1mm is the optimal depth within research parameter. The optimal depth has a great impact to the flow field. In laminar flow, transverse convection is an important method to disturb the flow boundary and enhance the mix between different fluid layers.

5.4. Effect of Different Dimple Spacing

Different dimple spacing is studied in this section and optimal dimple depth 0.1mm is used in these models. Reynolds number is kept at 500. Table is the basic data summarized from cases with different dimple spacing. Thermal resistance and dimple spacing has a linear relation: small dimple spacing allows placing more dimples and gains advantages to heat transfer enhancement. Pressure drop and dimple spacing also has a linear relation: smaller dimple spacing reduces the pressure loss.

Fig. 8 shows that the dimple has a limited impact area to the pressure loss. The influence will disappear at about 0.1mm downstream of dimple. The pressure drop will decrease when the dimple spacing increases and dimple number reduced. Fig. 13, Fig. 14 and Fig. 15 show the average local Nusselt number along *x* direction in the cases of different dimple spacing. The influence of dimple

to heat transfer also has a limited impact area. In Fig. 13, the influence to local Nusselt number will disappear at 1.2mm downstream of the dimple.

According to the analysis above, the influence of multiple dimple is simple addition of single dimples. Decreasing the spacing does not have important influence on the heat sink performance, and adding more dimples is an effective way to enhance the overall performance of heat sink.

6. CONCLUSIONS

Three geometric parameters - aspect ratio, dimple depth, dimple spacing- have been studied in this paper under constant Reynolds number 500 to find optimal geometric shape and study the flow field change caused by dimples. Below conclusions are obtained:

1. The influence of channel aspect ratio and dimple depth depends on the ratio of dimple depth and channel height d/H_c.

2. When d/H_c <0.6, vortex in the dimple is quite uniform and stays in the bottom part of dimple. With aspect ratio grows and d/H_c >0.6, vortex developed into two symmetrical ones and occupied most volume of dimple.

3. Existence of dimple causes transverse convection flow in the channel: two symmetric swirling while d/H_c <0.6 and four symmetric swirling while d/H_c >0.6, these swirling are the main reason of heat transfer enhancement.

4. The low velocity vortex in the dimple causes the velocity gradient decrease near wall compared to flat case. Dimple structure can reduce the pressure loss.

5. The influence of dimple on viscous dissipation and local Nusselt number disappears downstream of dimple after 0.1mm and 1.2mm, respectively. Effect of multiple dimples is the same as the sum of single dimple.

The transverse convection caused by dimple is very important to enhance the convection heat transfer under laminar flow. Besides the heat transfer enhancement, dimple can also reduce the pressure loss. It is an effective method to improve overall performance of microchannel heat

sink. In the study, optimal d/H_c is about 0.6, bringing 3.2K temperature decrease of maximum temperature. This can be enhanced by increasing the dimple number. The work in our paper provides reference for optimal design of dimple structure in microchannel heat sink.

ACKNOWLEDGMENT

The work was supported by the National Natural Science Foundation of China [51206187, 51306211] and Fundamental Research Funds for the Central Universities [No. 14CX05027A].

NOMENCLATURE

α	channel aspect ratio
ρ	density, kg/m^3
λ	thermo conductivity, W/m·K
μ	dynamic viscosity, Pa·s
ϕ	viscous dissipation rate, W/mm^3
ν	kinematic viscosity, m^2/s
λ	thermo conductivity, W/m·K
Δp	pressure drop, Pa
A_c	inlet cross-sectional area of the flow channel, mm^2
A	area, mm^2
c_p	isobaric heat capacity, J/K·kg
d	dimple depth, mm
D_e	equivalent diameter of channel, mm
H	heat sink height, mm
h	convective heat transfer coefficient, W/m^2·K
H_c	channel height, mm
H_w	channel width, mm
h_w	local convective heat transfer coefficient, W/m^2·K
L	channel length, mm
L_h	length of heating source, mm

Nu	Nusselt number
p	pressure, Pa
P	perimeter of the flow channel at inlet, mm
PF	performance factor
Q	total heat power of heating surface, W
q	heat flux, W/mm^2
r	dimple radius, mm
R	thermal resistance, K/W
Re	Reynolds number, $U_{in}.D_e/\nu$
s	dimple spacing, mm
T	temperature, K
U	velocity magnitude, m/s
u,v,w	dimensionless velocity components in x, y and z directions
x,y,z	cartesian coordinates

Subscripts

0	flat channel
f	fluid
heat	heating region
in	inlet
max	maximum
out	outlet

P	point *P* on fluid solid interface
s	solid
wall	fluid solid interface
x	slice at *x* location

REFRENCES

[1] http://www.itrs2.net/2012-itrs.html, 2016.

[2] D. B. Tuckerman, R. F. W. Pease, High-performance heat sinking for VLSI, Electron Device Letters IEEE 2 (5) (1981) 126–129.

[3] H. Y. Wu, P. Cheng, Friction factors in smooth trapezoidal silicon microchannels with different aspect ratios, International Journal of Heat and Mass Transfer 46 (14) (2003) 2519–2525.

[4] H. Y. Wu, P. Cheng, An experimental study of convective heat transfer in silicon microchannels with different surface conditions, International Journal of Heat and Mass Transfer 46 (14) (2003) 2547–2556.

[5] G. Hetsroni., A. Mosyak, E. Pogrebnyak, L. P. Yarin, Fluid flow in micro-channels, International Journal of Heat and Mass Transfer 48 (10) (2005) 1982–1998.

[6] G. Hetsroni., A. Mosyak, E. Pogrebnyak, L. P. Yarin, Heat transfer in micro-channels: comparison of experiments with theory and numerical results, International Journal of Heat and Mass Transfer 48 (25) (2005) 5580–5601.

[7] T. Y. Lin, S. G. Kandlikar, A theoretical model for axial heat conduction effects during single-phase flow in microchannels, Journal of Heat Transfer 134 (2) (2012) 020902.

[8] G.B. Zhou, S. C. Yao, Effect of surface roughness on laminar liquid flow in micro-channels, Applied Thermal Engineering 31 (2) (2011) 228–234.

[9] L. Gong, K. Kota, W. Q. Tao, Y. Joshi, Parametric numerical study of flow and heat transfer in microchannels with wavy walls, Journal of Heat Transfer 133 (2011) 051702.

[10] Y. Sui, P. S. Lee, C. J. Teo, An experimental study of flow friction and heat transfer in wavy microchannels with rectangular cross section, International Journal of Thermal Sciences 50 (12) (2011) 2473–2482.

[11] Y. Sui, C. J. Teo, P. S. Lee, Direct numerical simulation of fluid flow and heat transfer in periodic wavy channels with rectangular cross-sections, International Journal of Heat and Mass Transfer 55 (1) (2012) 73–88.

[12] Y. Sui, C. J. Teo, P. S. Lee, Y. T. Chew, C. Shu, Fluid flow and heat transfer in wavy microchannels, International Journal of Heat and Mass Transfer 53 (13) (2010) 2760–2772.

[13] S. L. Xu, W. J. Wang, K. Fang, C.N. Wong, Heat transfer performance of a fractal silicon microchannel heat sink subjected to pulsation flow, International Journal of Heat and Mass Transfer 81 (2015) 33–40.

[14] X. F. Yu, C. P. Zhang, J. T. Teng, S.Y. Huang, S. P. Jin, Y. F. Lian, C. H. Cheng, A study on the hydraulic and thermal characteristics in fractal tree-like microchannels by numerical and experimental methods, International Journal of Heat and Mass Transfer 55 (25) (2012) 7499–7507.

[15] L. J. Wang, W. Wu, X. Li, Numerical and Experimental Investigation of Mixing Characteristics in the Constructal Tree-Shaped Microchannel. International Journal of Heat and Mass Transfer 67 (2013) 1014–1023.

[16] C. B. Zhang, Y. P. Chen, M. H. Shi, Effects of roughness elements on laminar flow and heat transfer in microchannels, Chemical Engineering and Processing: Process Intensification 49 (11) (2010) 1188–1192.

[17] J. Cui, Y. B. Fu, A numerical study on pressure drop in microchannel flow with different bionic micro-grooved surfaces, Journal of Bionic Engineering 9 (1) (2012) 99–109.

[18] Y. Liu, J. Cui, Y. X. Jiang, W. Z. Li, A numerical study on heat transfer performance of microchannels with different surface microstructures, Applied Thermal Engineering 31 (5) (2011) 921–931.

[19] L. Guo, H. J. Xu, L. Gong, Influence of wall roughness models on fluid flow and heat transfer in microchannels, Applied Thermal Engineering 84 (2015) 399–408.
[20] J. Lee, K.-S. Lee, Correlations and shape optimization in a channel with aligned dimples and protrusions, International Journal of Heat and Mass Transfer 64 (5) (2013) 444–451.
[21] O. Alshroof, J. Reizes, V. Timchenko E. Leonardi, Flow structure and heat transfer enhancement in laminar flow with protrusion-dimple combinations in a shallow rectangular channel, Proceedings of the ASME 2009 Heat Transfer Summer Conference, 2009
[22] C. Bi, G.H. Tang, W.Q. Tao, Heat transfer enhancement in mini-channel heat sinks with dimples and cylindrical grooves, Applied Thermal Engineering 55 (2013) 121–132.
[23] X. J. Wei, Y. K. Joshi, P. M. Ligrani, Numerical simulation of laminar flow and heat transfer inside microchannel with one dimpled surface, Journal of Electronic Packaging, 129 (2007) 63-70.
[24] J. B. Lan, Y. H. Xie, D. Zhang, Flow and heat transfer in microchannels with dimples and protursions, Journal of Heat Tranfer 134 (2012) 021901.
[25] M. W. Ge, C. X. Cui, G. X. Cui, Study on flow structures due to a dimple in channel flow by direct numerical simulation, International Journal of Flow Control 4 (1) (2012) 61–82.
[26] H. Lienhart, M. Breuer, C. Köksoy, Drag reduction by dimples?–a complementary experimental/numerical investigation. International Journal of Heat and Fluid Flow 29 (3) (2008) 783–791.
[27] J. Turnow, N. Kornev, V. Zhdanov, E. Hassel, Flow structures and heat transfer on dimples in a staggered arrangement, International Journal of Heat and Fluid Flow 35 (0) (2012) 168–175.
[28] S.A. Isaev, N. V. Kornev, A. I. Leontiev, E. Hassel, Influence of the reynolds number and the spherical dimple depth on turbulent heat transfer and hydraulic loss in a narrow channel, International Journal of Heat and Mass Transfer 53 (1–3) (2010) 178–197.
[29] C.M. Tay, Y. T. Chew, B. C. Khoo, J. B. Zhao, Development of flow structures over dimples, Experimental Thermal and Fluid Science 52 (0) (2014) 278–287.
[30] C. Silva, E. Marotta, L. Fletcher, Flow structure and enhanced heat transfer in channel flow with dimpled surfaces: application to heat sinks in microelectronic cooling, Journal of Electronic Packaging 129 (2) (2007) 157–166.
[31] Y. H. Xie, H. C. Qu, D. Zhang, Numerical investigation of flow and heat transfer in rectangular channel with teardrop dimple/protrusion, International Journal of Heat and Mass Transfer 84 (0) (2015) 486–496.
[32] H. S. Yoon, S. H. Park, C. Y. Choi, M. Y. Ha, Numerical study on characteristics of flow and heat transfer in a cooling passage with a tear-drop dimple surface. International Journal of Thermal Sciences 89 (0) (2015) 121–135.

Table Caption List

Table 1 Effect of different aspect ratio

α	d/H_c	Δp/Pa	Δp_0/Pa	Nu	Nu_0	T_{max}	$\Delta p/\Delta p_0$	Nu/Nu_0	PF
1:1	0.2	2986.55	3062.91	8.21	8.12	351.20	0.98	1.01	1.02
2:1	0.4	9756.06	9867.43	8.52	8.15	349.33	0.98	1.05	1.05
3:1	0.6	23768.91	24178.25	9.11	8.16	343.95	0.98	1.12	1.12
4:1	0.8	47817.12	48724.98	9.44	8.23	339.39	0.98	1.15	1.16

Table 2 Effect of dimple depth

d/mm	d/H_c	Δp/Pa	T_{max}/K	R/(K/W)	Nu
Flat	0	48724.98	342.59	2.81	8.23
0.05	0.4	48338.51	340.66	2.61	9.04
0.10	0.8	47817.12	339.39	2.50	9.44
0.15	1.2	47055.63	339.90	2.61	9.42
0.20	1.6	46817.23	340.07	2.63	9.41

Table 3 Effect of different dimple spacing

s/mm	n	Δp/Pa	T_{max}/K	R/(K/W)	Nu
0.7	21	47817.12	339.39	2.50	9.44
1.0	15	48124.77	340.19	2.53	9.13
1.2	12	48323.04	340.35	2.54	9.02
1.6	9	48441.53	340.88	2.56	8.82
2.8	6	48558.86	341.51	2.60	8.61
Flat	0	48724.98	342.59	2.81	8.23

Figure Captions List

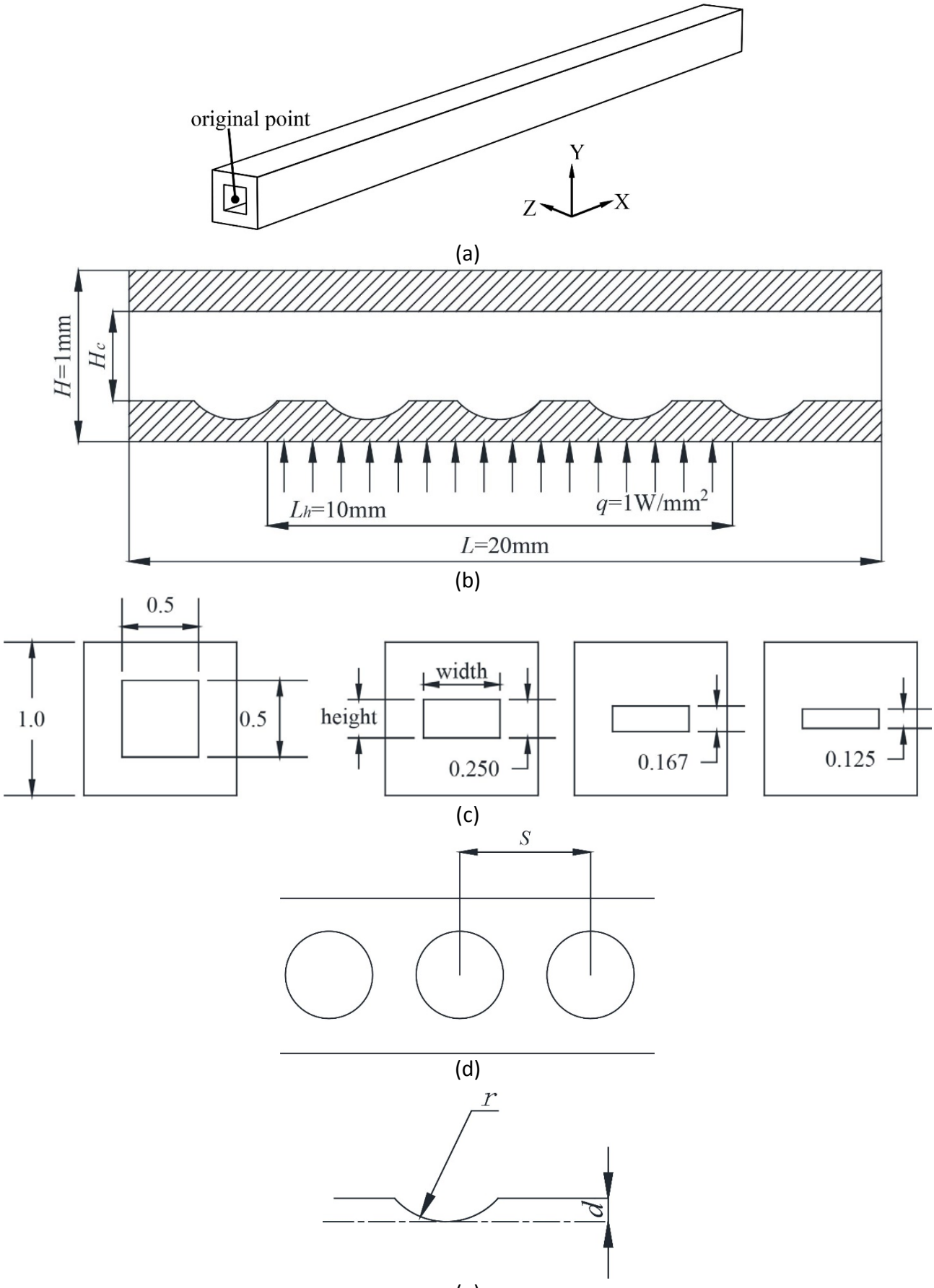

Fig. 1 Geometry models (a) 3D view (b) cross-section view (c) different aspect ratio (d) dimple spacing (e) dimple depth

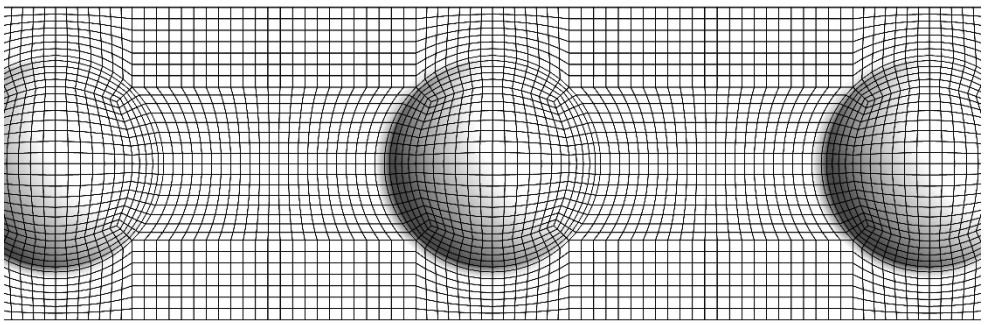

Fig. 2 Hexahedral mesh of one of the models

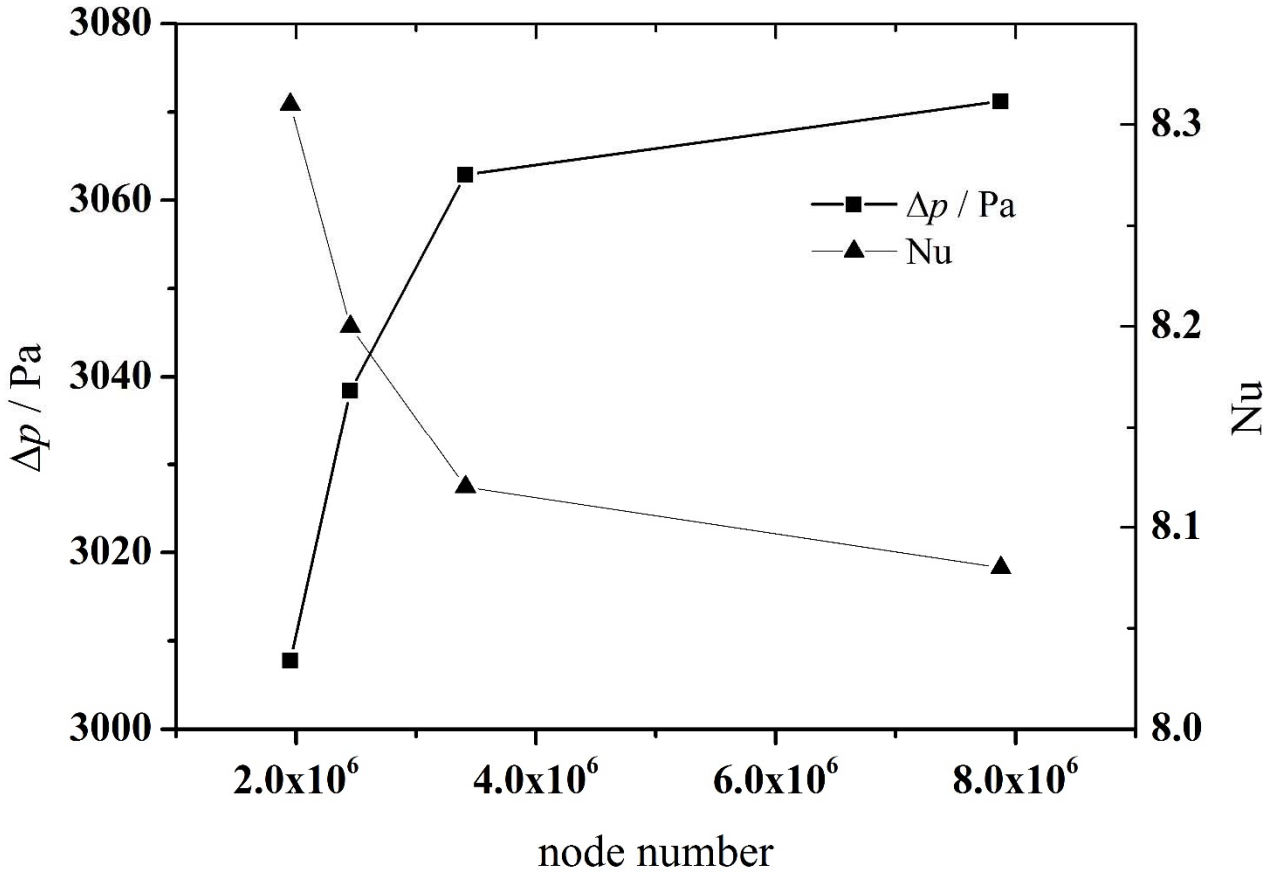

Fig. 3 Grid independency check

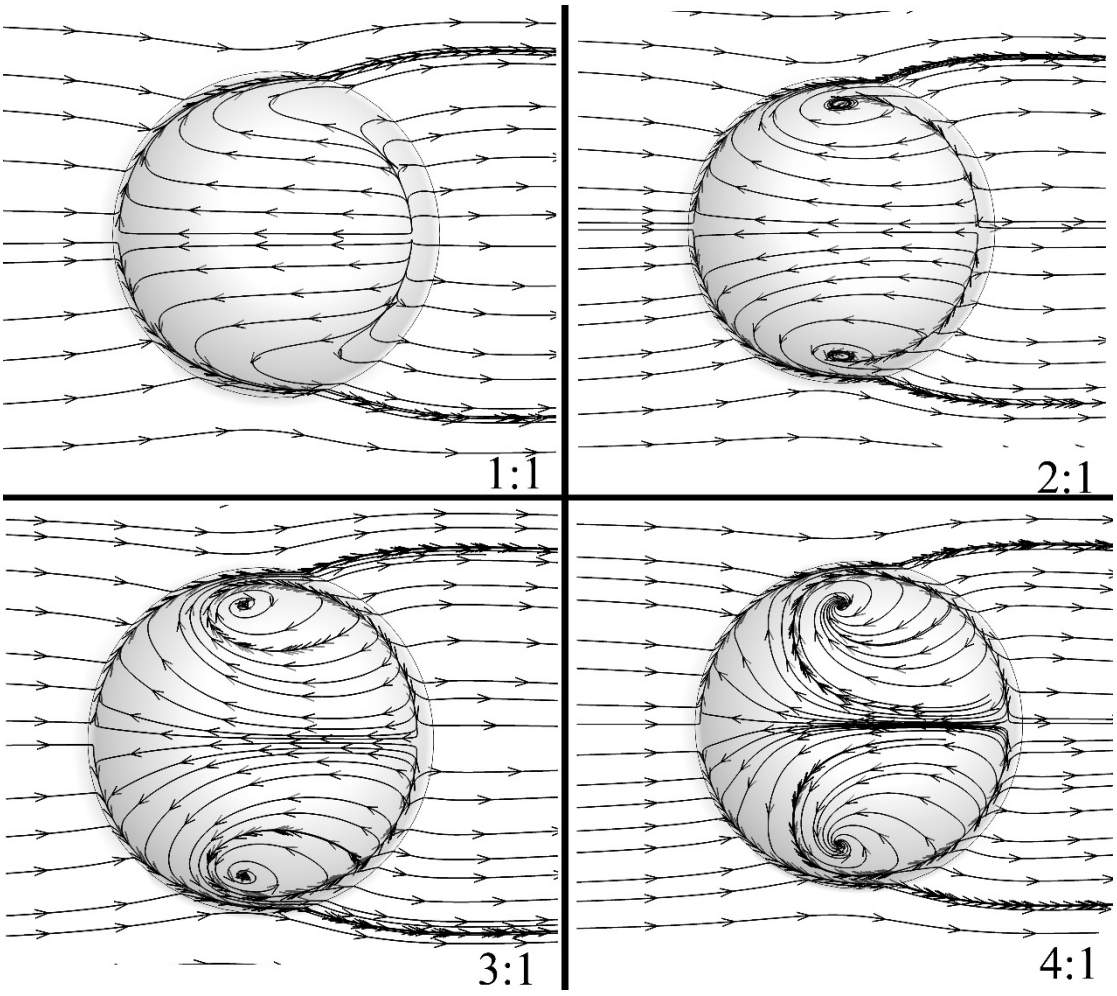

Fig. 4 Limited stream line near the dimple of different aspect ratio (+*y* view, *x*=10mm)

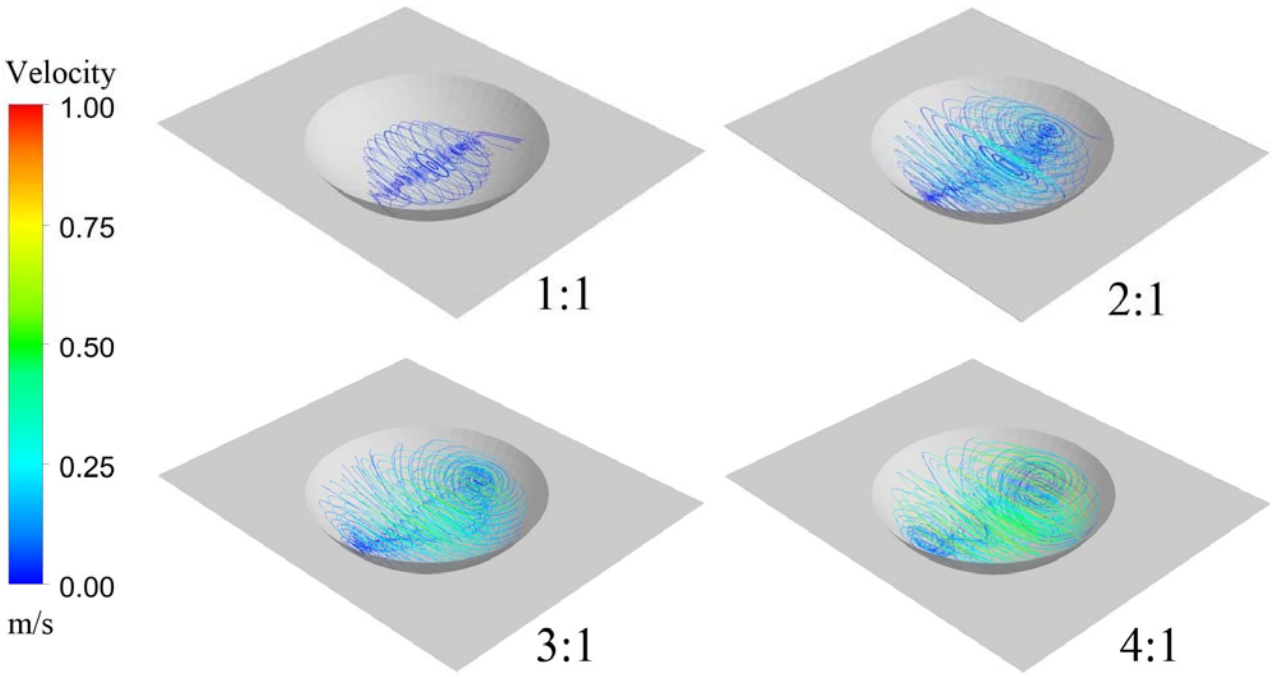

Fig. 5 Streamline in the dimple of different aspect ratio (*x*=10mm)

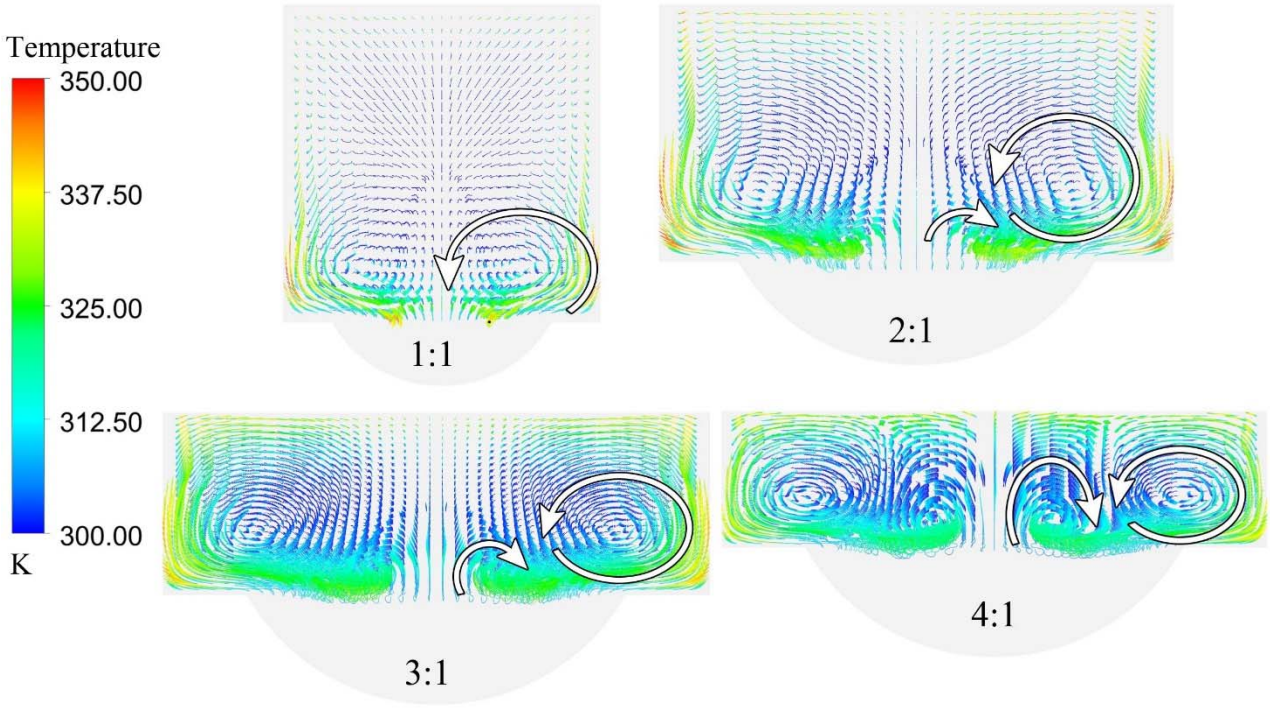

Fig. 6 Streamline view on positive *x* direction

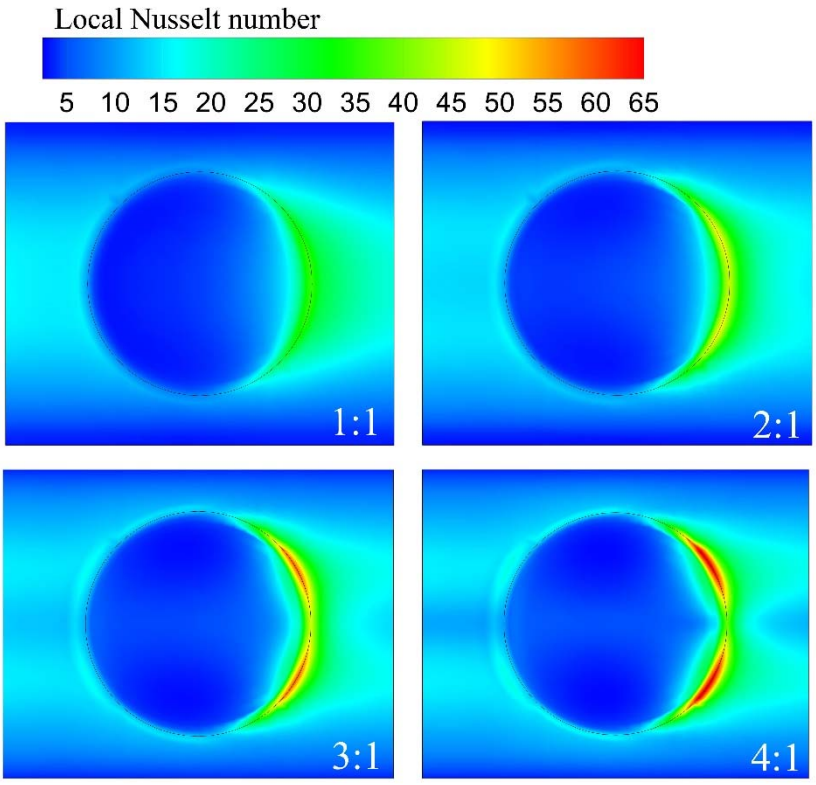

Fig. 7 Local Nusselt number of channel bottom (*x*=10mm)

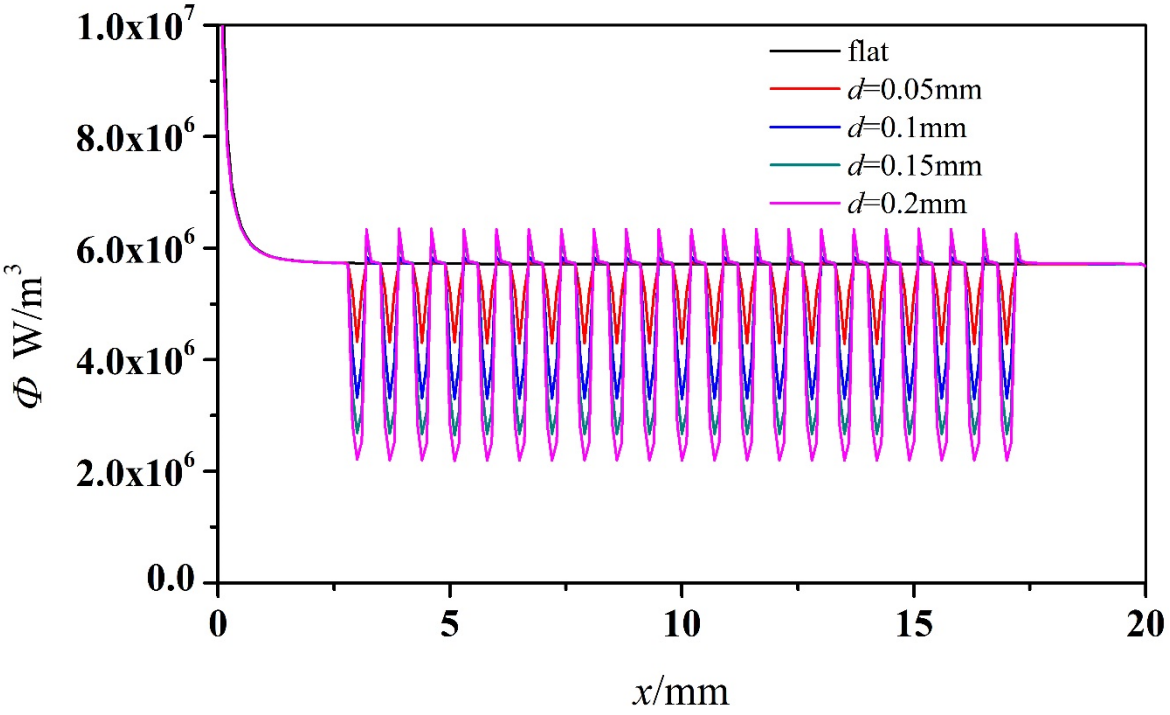

Fig. 8 Viscous dissipation along the *x* coordinate

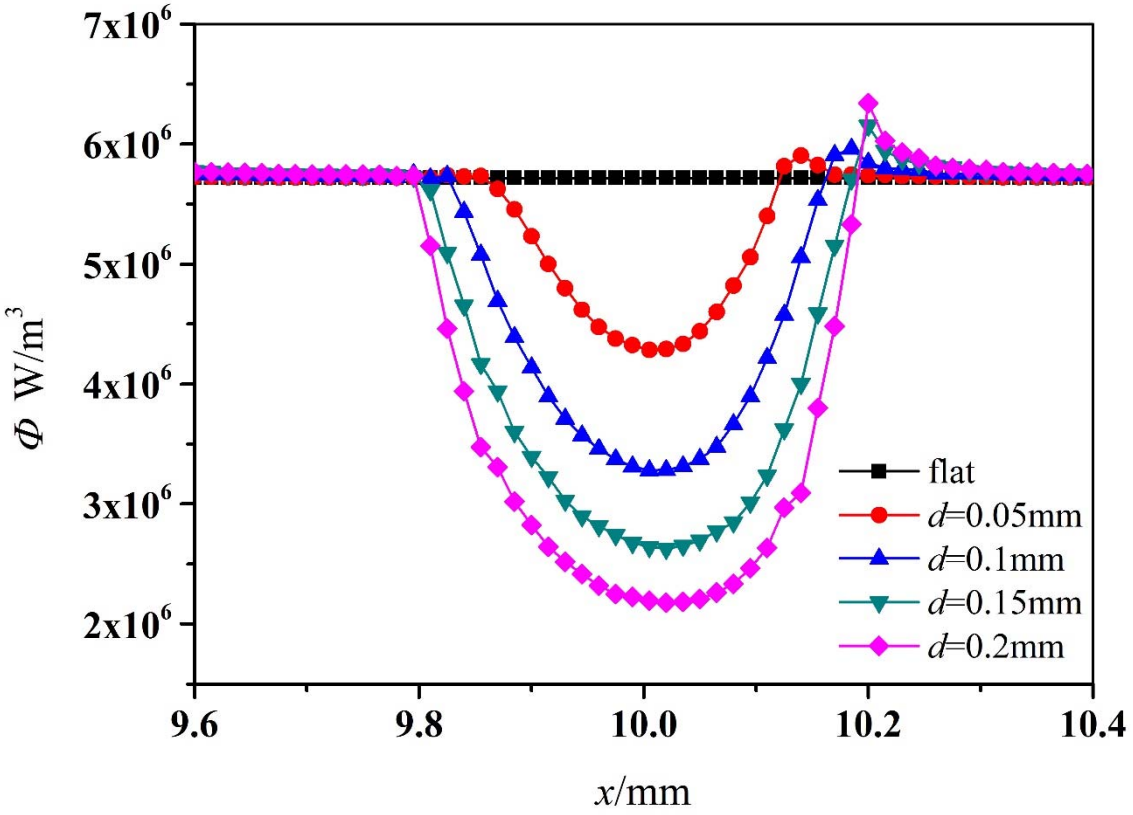

Fig. 9 Zoom in at *x*=10mm of Fig. 8

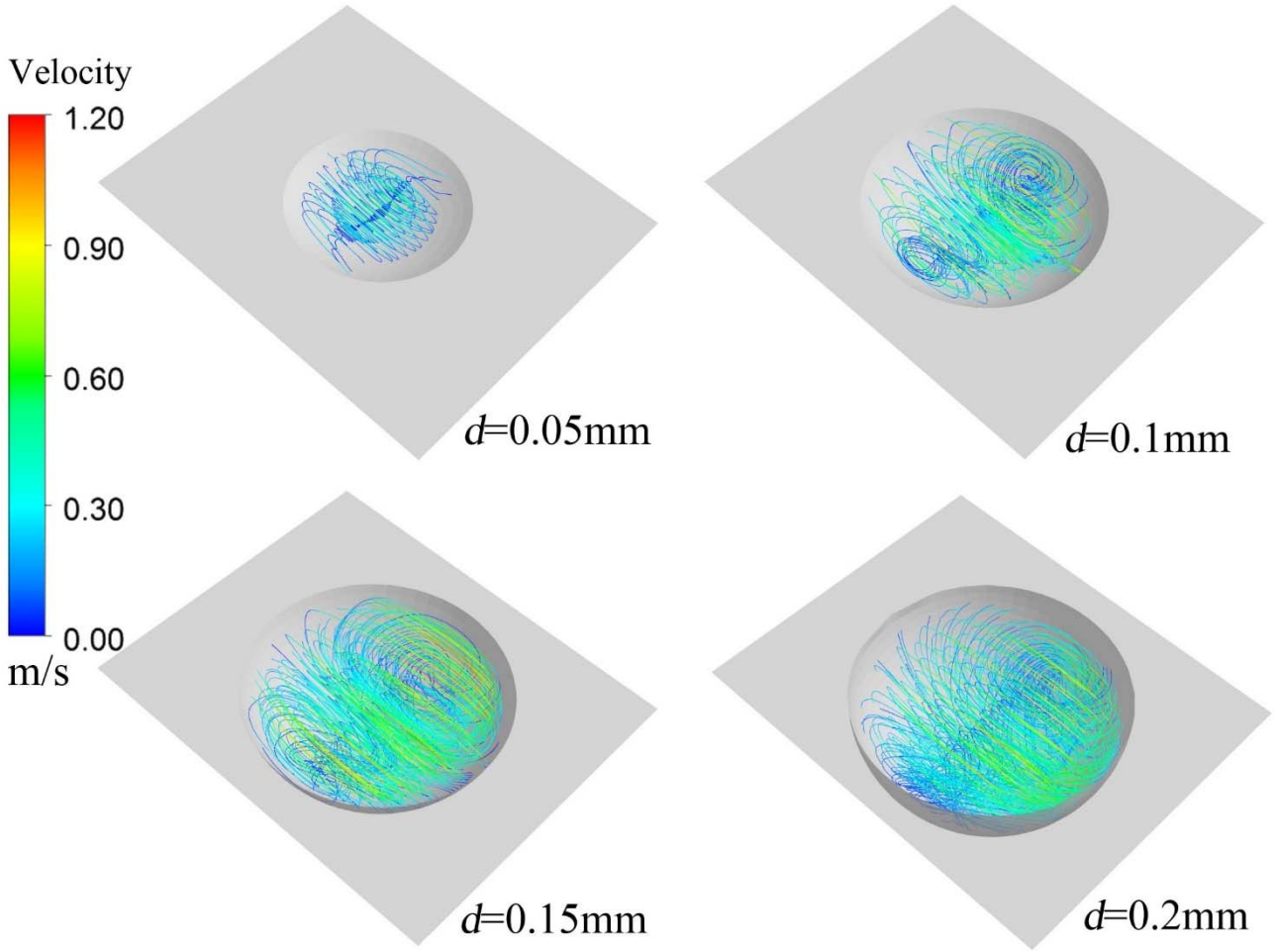

Fig. 10 Streamline in dimple with different dimple depth

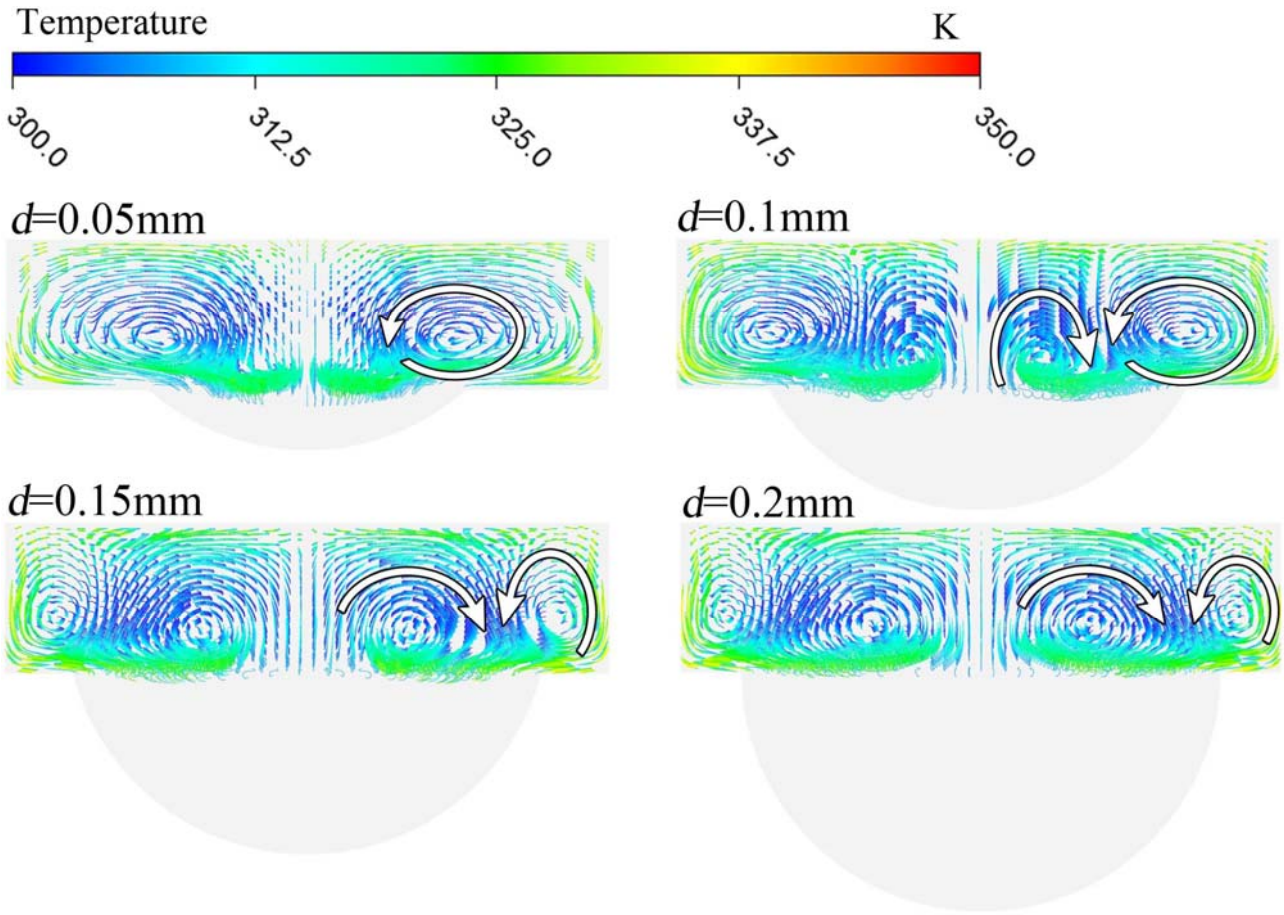

Fig. 11 Streamline view on positive *x* direction

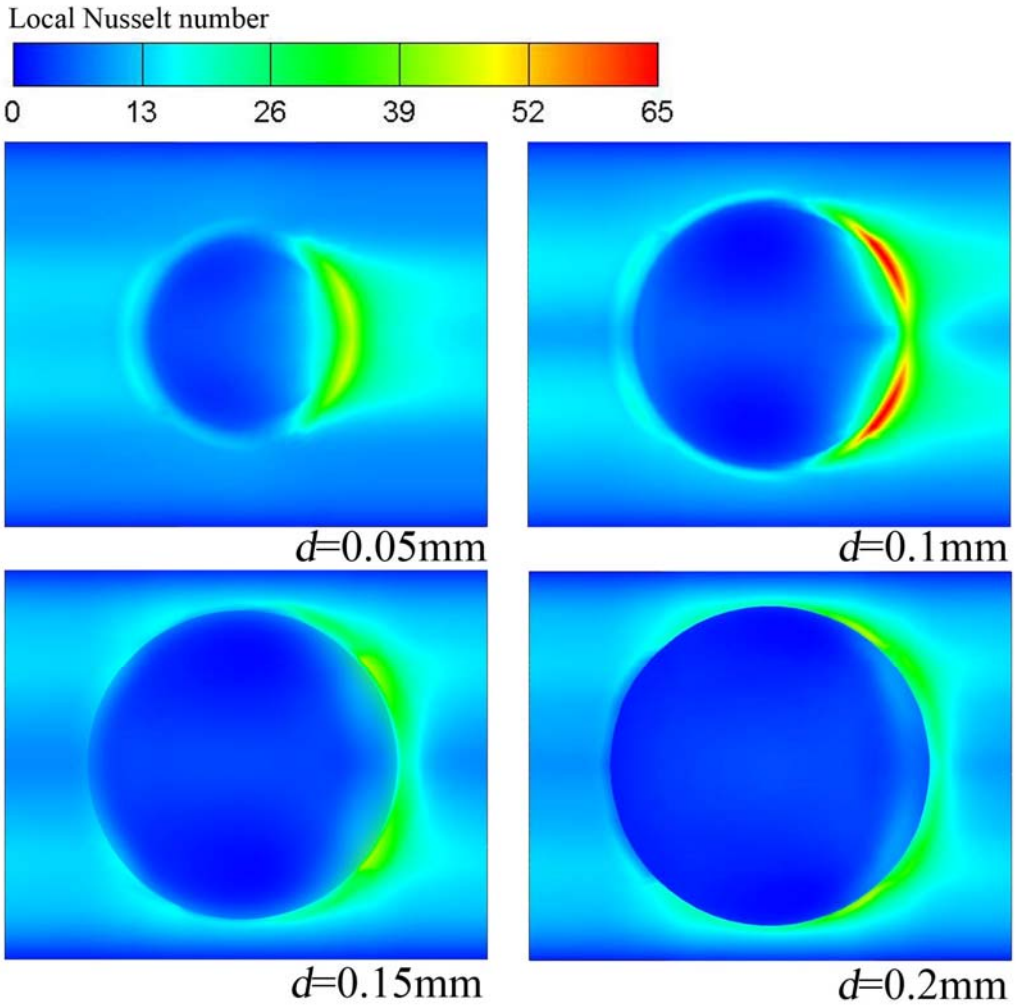

Fig. 12 Local Nusselt number of channel bottom (*x*=9.7-10.3mm)

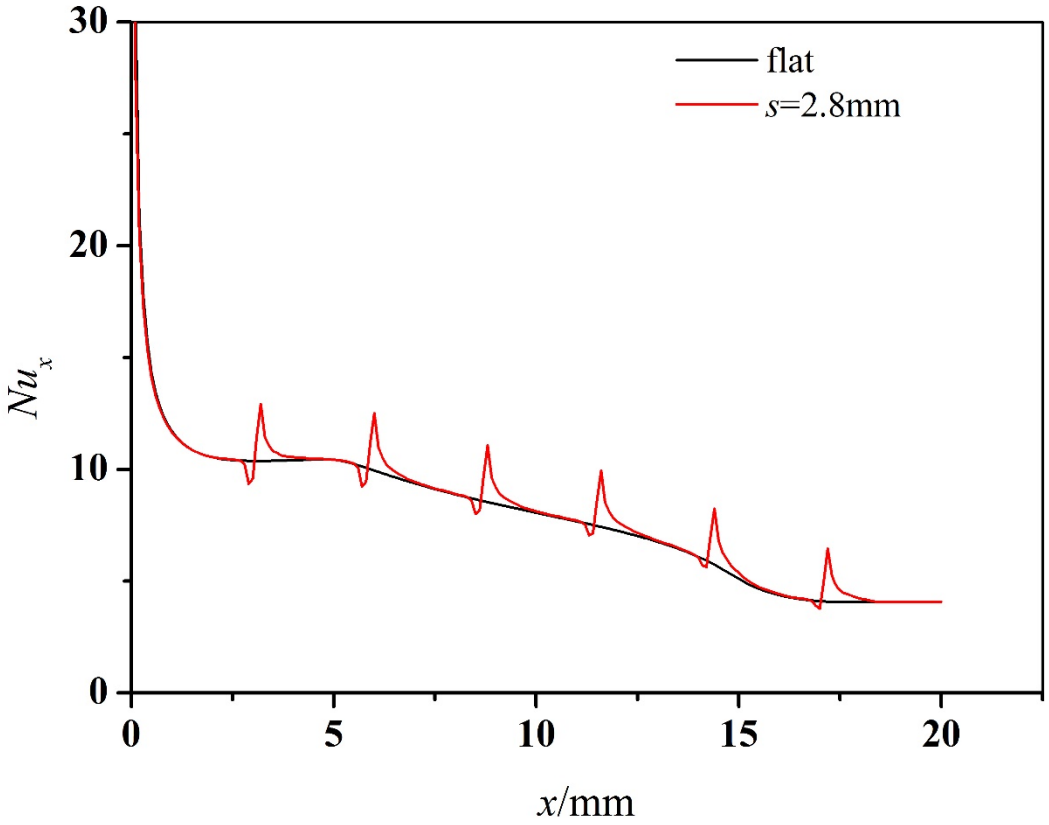

Fig. 13 Average local Nusselt number along *x* direction (*s*=2.8mm)

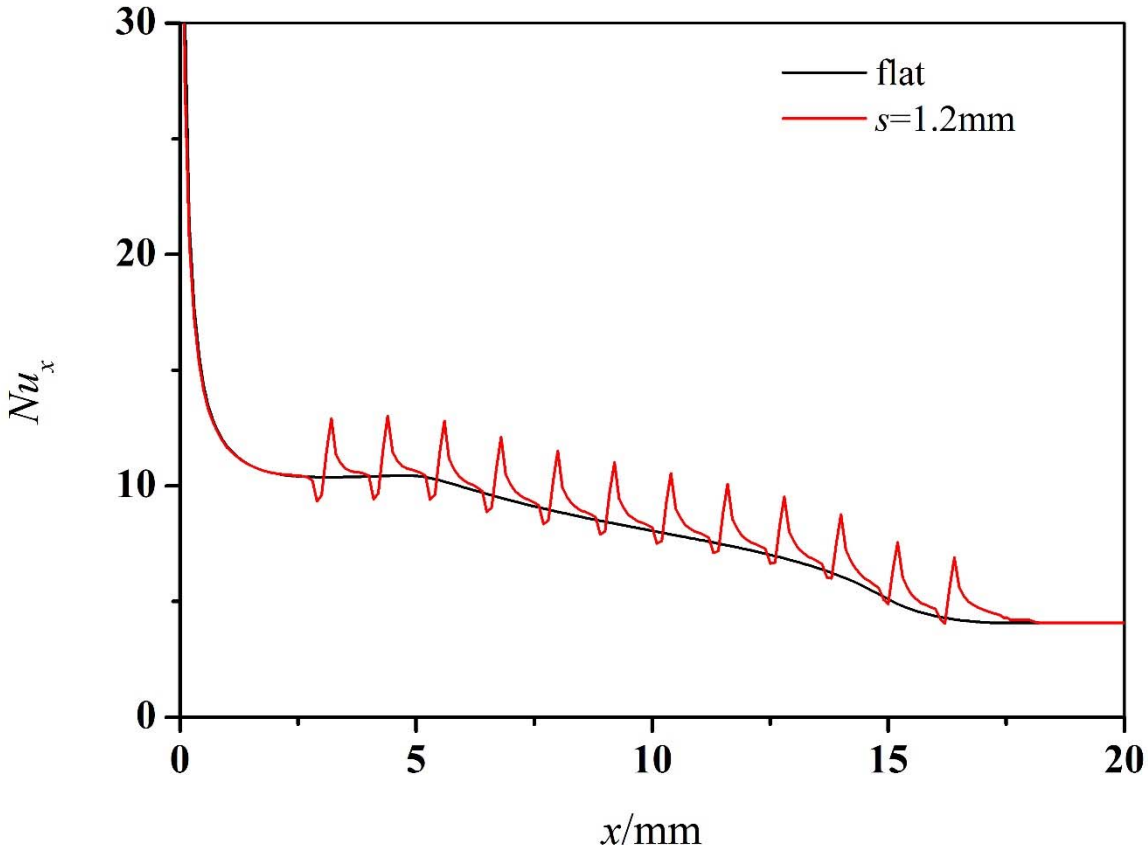

Fig. 14 Average local Nusselt number along *x* direction (*s*=1.2mm)

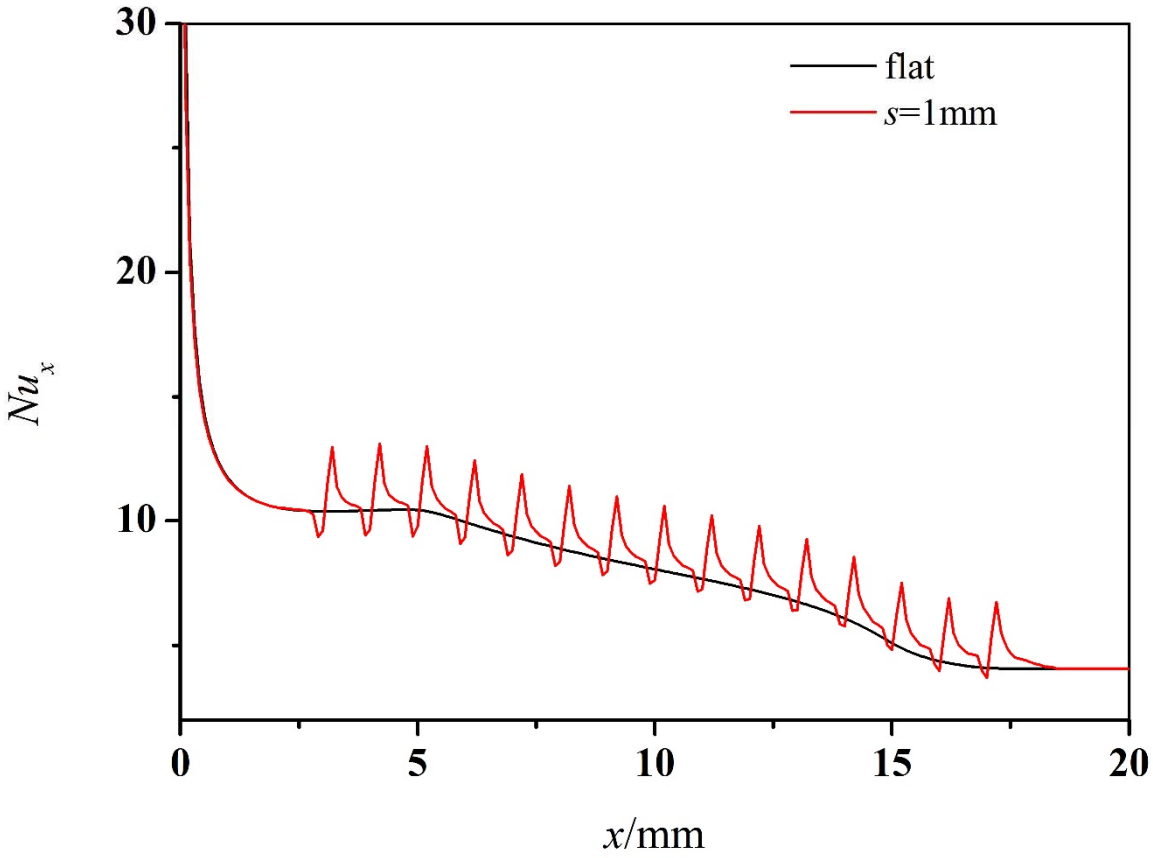

Fig. 15 Average local Nusselt number along *x* direction (*s*=1mm)